J Mater Sci: Mater Electron (2016) 27:12374–12384
DOI 10.1007/s10854-016-5104-2

Study of electrochemically grown copper indium diselenide (CIS) thin films for photovoltaic applications

Ashwini B. Rohom[1] · Priyanka U. Londhe[1] · Ganesh R. Bhand[1] · Manorama G. Lakhe[1] · Nandu B. Chaure[1]

Received: 22 December 2015 / Accepted: 30 May 2016 / Published online: 7 June 2016

Abstract CIS thin films have been grown electrochemically from an aqueous electrolyte at room temperature on fluorine doped tin oxide coated glass substrate at different deposition potentials ranging from −0.7 to −1.0 V versus Ag/AgCl reference electrode. Cyclic voltammetry was studied at slow scan rate to optimize the deposition potential. The thin film samples were selenized in a tubular furnace at 400 °C for 20 min. X-ray diffraction and Raman analysis was used to study the structural properties. Optical absorption, scanning electron microscopy and energy dispersive X-ray analysis (EDAX) have been used to investigate the band-gap, surface morphology and compositional analysis. Electrical properties were studied with the help of current–voltage measurements. Conductivity type for CIS thin films was studied by using photo-electrochemical study. The prominent reflections (112), (204/220) and (312/116) of tetragonal chalcopyrite CIS have been revealed for all as-grown and selenized samples. The energy band gap of the selenized CIS thin film deposited at various deposition potentials was found to be ∼1.03 to 1.24 eV. Granular, uniform and void free surface was observed in as-prepared sample, while large clusters were noticed in selenized samples. EDAX results reveal that the stoichiometric CIS thin film are deposited −0.8 V, however, Cu-rich and In-rich CIS layers were grown at lower and higher cathodic deposition potentials, deviated from −0.8 V. The values ideality factor (η) calculated from I–V measurements were found to be decreased upon selenization. The Raman spectra of stoichiometric CIS thin film shows dominant A1 mode with spectral features sensitive to the microcrystalline quality of the layers. A ordered defect compound layer and secondary phases of CuSe are observed in In-rich and Cu-rich CIS layers, respectively.

1 Introduction

Copper indium selenide (CIS) polycrystalline semiconductor is one of the most popular materials for thin film solar cell fabrication due to large mean free path and long diffusion length of minority carriers [1]. The direct energy gap of CIS results in large absorption coefficient, which in turn permits the use of thin layers (1–2 μm) of active materials. CIS based solar cells are also known for their long term opto-electronic stability and ability to undergo band-gap engineering (from 0.9 to 1.6 eV) by alloy formation like replacement of Se by S or by doping Ga and Al [2, 3]. Recently, the laboratory scale and module efficiency of CIGS based devices reached to 21.7 and 15.7 %, respectively [4].

The highest efficiencies of solar cells have been prepared by using vacuum based evaporation methods, which has various technical limitations like non-uniform evaporation of metal precursors at high temperature over large area, highly pure precursor material and capital investment. Sputtering technique is appropriate for large area deposition, however it requires sophisticated equipment along with vacuum and costly sputtering targets [5]. A great deal of efforts has been made to develop low cost techniques for preparation of CIS thin films such as electrodeposition [6, 7]. Electrodeposition method is potentially suitable method to obtain the low cost deposition of complex

✉ Nandu B. Chaure
n.chaure@physics.unipune.ac.in

[1] Electrochemical Laboratory, Department of Physics, Savitribai Phule Pune University, Pune 411007, India

metallic layers [8]. The electrodeposition process provides several advantages viz. negligible waste of chemicals, low equipment cost, high deposition rate, control on composition and thickness of material and deposition over large and arbitrary shaped area. Electrodeposition process is mainly controlled by several deposition parameters choice of precursor materials, compositional ratio of the precursor materials, solvents for processing, pH of solution, temperature, deposition potential and ambient used. Electrodeposition method has been successfully used for the deposition of elemental, binary, ternary and quaternary compounds [9–12]. In general, two procedures have been employed to deposit CIS layers, first, the co-deposition of Cu–In–Se [13] and other is deposition of Cu–In alloy and subsequent selenization [14]. One-step electrochemical method may offer a convenient way to deposit all the elements together at desirable growth potential which potentially lead to produce the stoichiometric CIS thin films [15]. Reports are also available on electrodeposition of CIS from aqueous [16] and non-aqueous [17, 18] electrolyte.

The electrodeposition of CIS was initiated by Bhattacharya [19] and subsequently Pottier et al. [20] have reported the growth of CIS by using complexing agent. The CIS based thin film solar cell devices with power conversion efficiency $\sim$5 to 6 % were produced by various groups [21–24]. Recently Bhattacharya et al. [25] has reported 14.1 % efficiency of CIGS solar cell using electrodeposition and 15.4 % in combination of electrodeposition with PVD technique [26].

In the present study we have used hydrion 3 pH buffer solutions to produce CIS layers. The dependence of the chemical composition, crystal structure, morphology, conductivity type etc., on the deposition potentials along with the electrochemistry of CIS system is explored.

2 Experimental details

2.1 Chemicals

All chemicals used for the electrodeposition of CIS thin films were purchased from Sigma-Aldrich of purity at least 99.9 % and used as-received. Fluorine doped tin oxide (FTO) coated glass substrates of sheet resistance 10–15 Ω/□ were purchased from Pilkington, UK. The double distilled deionized water was used as a solvent.

2.2 Electrodeposition of CIS thin films

Electrodeposition of CIS was performed potentiostatically with three electrode cell configuration. The reference, counter and working electrodes were Ag/AgCl, graphite and FTO coated glass substrate, respectively.

The electrolyte consists copper chloride ($CuCl_2$), indium chloride ($InCl_3$) and selenous acid ($H_2Se_2O_3$) (1:2:1 molecular ratio) dissolved in pH 3 hydrion buffer solution. Sulfamic acid and potassium hydrogen phthalate was used to prepare pH 3 hydrion buffer solutions in order to reduce the H^+ and OH^- ions present in the electrolyte. Lithium chloride (LiCl) is used as supporting electrolyte.

The electrochemistry of ternary Cu–In–Se system was studied by using cyclic voltammetry. The chronoamperometric measurements to electrodeposit CIS thin films were studied under potentiostatic condition for potentials ranging from −0.7 to −1.0 V. Immediately after deposition, the samples were thoroughly rinsed with warm water and dried in air ambient. The samples were selenized in Ar ambient to improve the crystallinity and particle size. Two step annealing was employed to selenize the samples. In the first step the samples were heated at 200 °C for 30 min to melt the Se ingots and secondly the temperature was maintained to 400 °C for 10 min, the temperature was then cooled naturally to room temperature. The as-grown and selenized CIS thin films electrodeposited at various deposition potentials were thoroughly studied.

2.3 Materials characterization

Cyclic voltammetry and the electrodeposition of CIS system was performed using μ3AUT 70762 AUTOLAB potentiostat/galvanostat. The structural properties were studied by means of X-ray diffraction (XRD), model Bruker D8 advance diffractometer with Cu Kα anode of wavelength 0.154 nm and Raman spectrophotometer model Invia Renishow with an excitation at 785 nm emission line. Optical absorption measurements were carried out by JASCO UV–Vis-NIR spectrometer. Surface morphology was studied with the help of JEOL JSM 6360A, scanning electron microscope with an operating voltage 20 kV. The elemental atomic percentage concentrations of samples were obtained by energy dispersive X-ray analysis technique equipped with the above SEM unit. The Potentiostat, SP 300 Biologic equipped with two probe measurement setup was employed to study the electrical properties. The conductivity type of CIS thin films was studied with photo-electrochemical (PEC) measurements. Three-electrode geometry was employed for PEC studies consisting graphite and Ag/AgCl as counter and reference electrode, respectively in 1 M KCl. The samples were illuminated with white light source of intensity $\sim$100 mW/cm^2.

3 Results and discussion

3.1 Electrochemistry of the CIS system: cyclic voltammetry and chronoamperometry

3.1.1 Cyclic voltammetry of CIS system

The electrodeposition of CIS was performed in presence of desired amount of precursor's concentration and hydrion pH 3 buffer solutions [27]. The cyclic voltammogram (CV) recorded in presence of Cu, In and Se ions with hydrion buffer 3 solution at 5 mV/s scan rate is depicted in Fig. 1.

Initially, at lower cathodic potentials up to −0.4 V, the features noticed are assigned to the reduction of Cu and Se by the following charge-transfer reactions marked as region 'A',

$$Cu^{2+} + 2e^- = Cu \quad Eo = +0.34\,V \text{ versus SHE} \tag{1}$$

$$H_2SeO_3 + 4e^- + 4H^+ = Se + 3H_2O \quad Eo = +0.74\,V \text{ versus SHE} \tag{2}$$

Metallic In is proposed to be electrodeposited by the following charge transfer reaction;

$$In^{3+} + 3e^- = In \quad Eo = -0.34\,V \text{ versus SHE} \tag{3}$$

The plateau region observed (marked as 'B') is assigned to the diffusion controlled electrodeposition which could be suitable for the synthesis of polycrystalline and controlled stoichiometric CIS thin films. The sharp rise in the cathodic current observed at −0.95 V is due the hydrogen evolution as well as the metallic deposition of In.

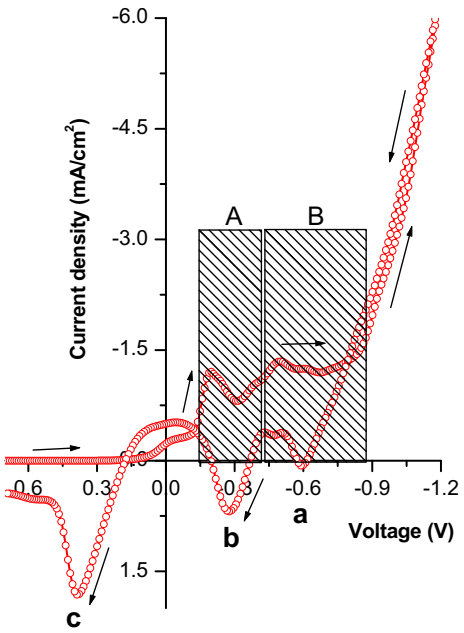

Fig. 1 Cyclic voltammogram recorded in presence of Cu, In and Se precursors at 5 mV/s with respect to Ag/AgCl reference electrode

The electrodeposition of CIS takes place by following reaction;

$$Cu^{2+} + In^{3+} + 2SeO_3^{2-} + 9e^- + 12H^+ = CuInSe_2 + 6H_2O \tag{4}$$

The stripping peaks correspond to In, Cu and Se attributed during the anodic scan and marked as 'a', 'b' and 'c', respectively.

Note that the potassium compound used in pH 3 hydrion buffer and LiCl used as supporting chemicals, produces the K^+ and Li^+ ions in reaction matrix. The equilibrium reduction potentials of K and Li are −2.93 and −3.05 V with respect to SHE by the following charge transfer reaction

$$K^+ + e^- \rightarrow K_{(S)} \quad -2.93\,V \text{ versus SHE} \tag{5}$$

$$Li^+ + e^- \rightarrow Li_{(S)} \quad -3.05\,V \text{ versus SHE} \tag{6}$$

These ions in the electrolyte are utilized only to increase the conductivity to electrodeposit the desired amount of Cu, In and Se ions onto working electrode. The applied potentials were −0.7 to −1.0 V therefore K and Li are not electrodeposited. Furthermore the K and Li were not detected in the compositional analysis.

3.1.2 Chronoamperometry for CIS thin films

Chronoamperometric analysis for CIS thin films was performed on to CIS samples deposited at −0.7 V (a), −0.8 V (b), −0.9 V (c) and −1 V (d) are shown in Fig. 2. Inset shows the magnified image for the curve (a). The Chronoamperometric curve shows the current density increases with increase in growth potentials.

The steady-state current is given by

$$I = 4nDFca \tag{7}$$

where, 'D' is the diffusion coefficient, 'a' is the area, 'c' is the concentration, 'F' is the Faraday constant and 'n' is the number of electrons transferred per molecule. Each curve confirms the diffusion controlled growth with instantaneous nucleation. The rapid decay observed initially is proposed due to the charging/discharging of double layer [28].

3.2 Structural properties: XRD and Raman studies

3.2.1 XRD analysis

The XRD pattern of as-grown and selenized CIS thin films are shown in the Fig. 3A, B, respectively. The prominent three reflections (112), (220/204) and (116/312) of

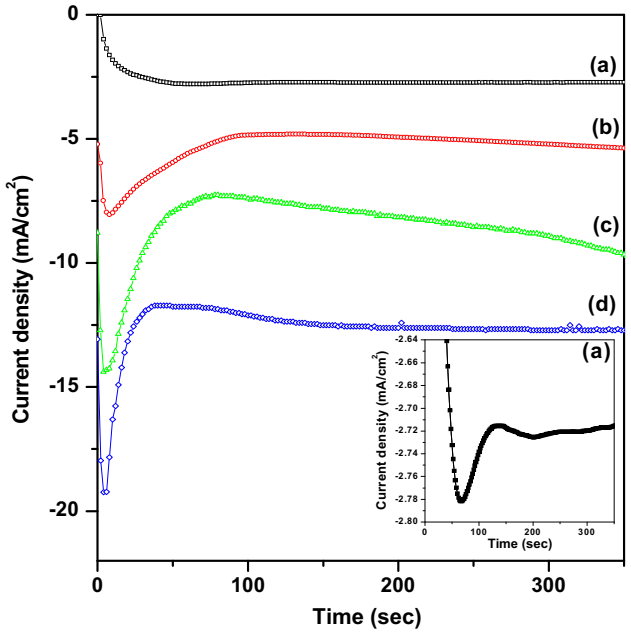

Fig. 2 Chronoamperometric curves for CIS thin films grown at *a* −0.7 V, *b* −0.8 V, *c* −0.9 V and *d* −1 V. *Inset* shows the magnified curve for CIS thin film electrodeposited at −0.7 V

tetragonal structure of CIS are attributed for both as-grown and selenized samples. It is noteworthy that the, metallic or secondary phases were not observed in the sample deposited at −0.8 V, where as the peaks related to In_XSe_Y along with CIS were observed in the sample deposited at −0.9 and −1 V. The peaks attributed to FTO and In_XSe_Y are marked as solid circles and hollow circles, respectively. Small humps observed in XRD pattern of the CIS sample deposited at −0.7 V is associated to CuSe. The enhancement in the crystallinity is observed in all samples after selenization. The results obtained from XRD analyses are tabulated in Table 1.

3.2.2 *Raman analysis*

The CIS layers were further analyzed by Raman spectroscopy to understand the more structural details. Figure 4 shows the Raman spectra of as-grown and selenized CIS thin films deposited from −0.7 V (a), −0.8 V (b), −0.9 V (c) and −1 V (d). The formation of ternary CIS phase is clearly identified by three peaks. The most intense peak observed at 170 cm^{-1} for all samples is assigned to the

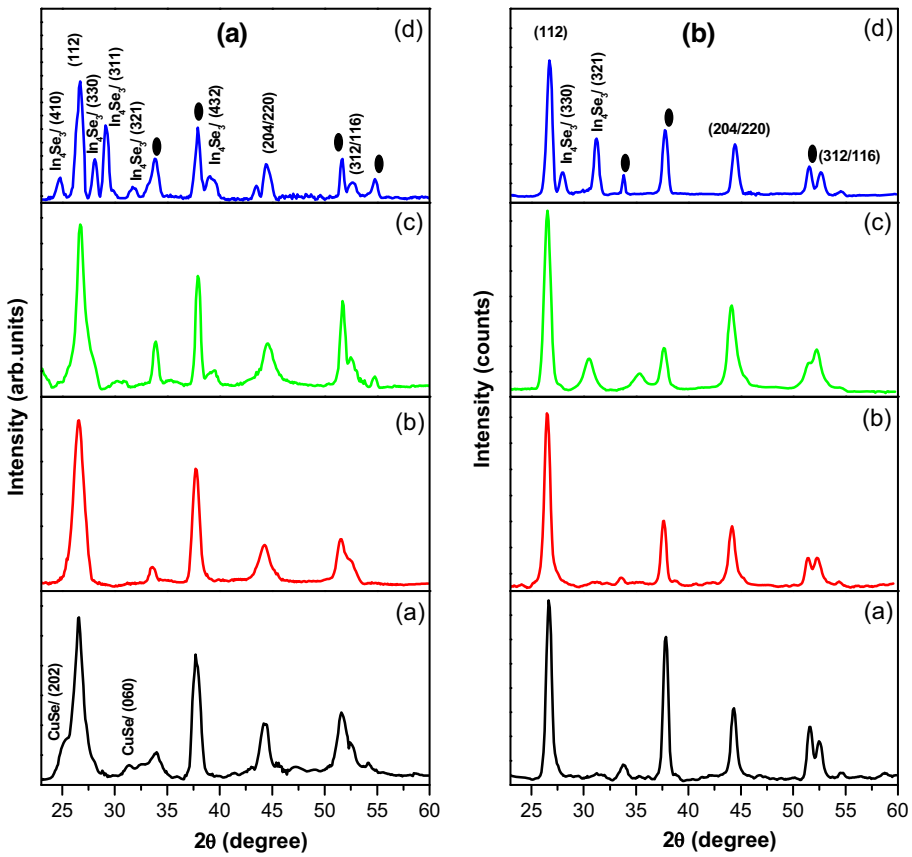

Fig. 3 **A** XRD patterns for as-grown CIS thin films deposited at various deposition potentials −0.7 V (*a*), −0.8 V (*b*), −0.9 V (*c*) and −1 V (*d*) with respect to Ag/AgCl reference electrode. Peaks related to FTO are *marked* as a *solid circle*. **B** XRD patterns for selenized CIS thin films deposited at various deposition potentials −0.7 V (*a*), −0.8 V (*b*), −0.9 V (*c*) and −1 V (*d*). Peaks related to FTO are *marked* as a *solid circle*

Table 1 A summary of XRD results obtained from as-grown and selenized CIS layers deposited for different deposition potentials

Deposition potentials	2θ (°)			d (Å)			FWHM (°)		Miller indices
	Observed		Standard	Observed		Standard	Observed		
	As-grown	Selenized		As-grown	Selenized		As-grown	Selenized	
−0.7 V	26.55	26.63	26.62	3.362	3.344	3.345	0.664	0.506	(111)
	44.44	44.36	44.28	2.037	2.039	2.043	0.752	0.563	(204/220)
	52.64	52.47	52.41	1.738	1.742	1.744	0.889	0.618	(116/312)
−0.8 V	26.54	26.48	26.62	3.355	3.361	3.345	0.998	0.557	(111)
	44.28	44.30	44.28	2.043	2.042	2.043	1.021	0.685	(204/220)
	52.60	52.31	52.41	1.738	1.746	1.744	1.133	0.907	(116/312)
−0.9 V	26.69	26.53	26.62	3.362	3.355	3.345	0.762	0.589	(111)
	44.42	44.12	44.28	2.037	2.050	2.043	0.996	0.826	(204/220)
	52.47	52.35	52.41	1.742	1.745	1.744	1.037	0.923	(116/312)
−1 V	26.68	26.69	26.62	3.337	3.336	3.345	0.629	0.493	(111)
	44.32	44.36	44.28	2.041	2.039	2.043	0.689	0.557	(204/220)
	52.62	52.55	52.41	1.7137	1.739	1.744	0.711	0.576	(116/312)

characteristics A1 mode of the chalcopyrite CIS phase. The peaks observed at 207 and 224 cm^{-1} are associated to E and B2 modes of CIS phase [29]. The strong peak appeared at 260 cm^{-1} in Fig. 4a is related to the secondary phase of CuSe. This peak is not observed in the sample deposited at higher potentials. This agrees well with XRD result. The presence of CuSe phases are highly conductive, which may produce shunt paths and detrimental to the efficiency of CIS solar cell. The Raman peaks observed in sample (b) deposited at −0.8 V are corresponds to CIS only. The features related to In_XSe_Y were not observed for the sample deposited at higher growth potentials (−0.9 and −1 V), however the formation of ordered defect compound (ODC) of the CIS phase was obtained at 150 cm^{-1}. The formation of ODC layer could be associated with EDAX analyses which obtained low Cu/In ratio. When the CIS films are In-rich/Cu-deficient then formed surface layer is known as ordered defect compound (ODC). This ODC layer has n-type conductivity. Cu vacancy (V_{Cu}^{-}) is the most dominated defect due to very low formation energy, which is a consequence of the anti-bonding Cu–Se hybrid state at the valence band [30]. The peak appeared at 150 cm^{-1} in Raman spectra for CIS thin films confirms the presence of ODC layer formation. Witte et al. reported the Raman analysis of CIGS thin films with various copper content. They observed a shoulder at around 150 cm^{-1} in all Cu-poor absorber layer in Raman spectra due to presence of ODC phase [31]. Marquez et al. [32] report all physical parameters including band structure, defects, effective mass of carriers, dielectric constant, activation energy, etc. for ODC layer. The ODC layer may be useful for the development of high efficiency solar cell devices [33]. The peak appeared at 118 cm^{-1} observed in all Raman spectra's belongs to the laser line which was used for the calibration of Raman wave number.

3.3 Optical properties

The optical absorption measurements were carried out with the help of a UV–Vis spectrophotometer in the wavelength region 600–1000 nm is depicted in Fig. 5. The energy band-gap values were estimated by extrapolating the straight line segment of the graph $(\alpha h\upsilon)^2$ versus $h\upsilon$, to the x-axis. The energy band-gap values for as-deposited samples electrodeposited at −0.7 to −1 V were estimated in the range of 1.03–1.24 eV. The energy band-gap of CIS layers decreases upon selenization. The reduction in the band-gap after selenization may be due to the recrystallization and increase in the particle size. A systematic change in the band-gap towards uphill direction was observed for the sample deposited from lower to higher growth potentials. The large band-gap estimated at higher potentials could be associated to small grain size of the deposit and/or the growth of stoichiometric layer. The estimated values of the band-gap are summarized in Table 2 which are in good agreement with the reported value [7].

3.4 Surface properties and compositional analysis: SEM and EDAX

3.4.1 SEM analysis

The SEM images of as-prepared and annealed CIS layers grown at −0.7 to −1 V are shown in Fig. 6. No significant change in surface morphology of as-prepared CIS with

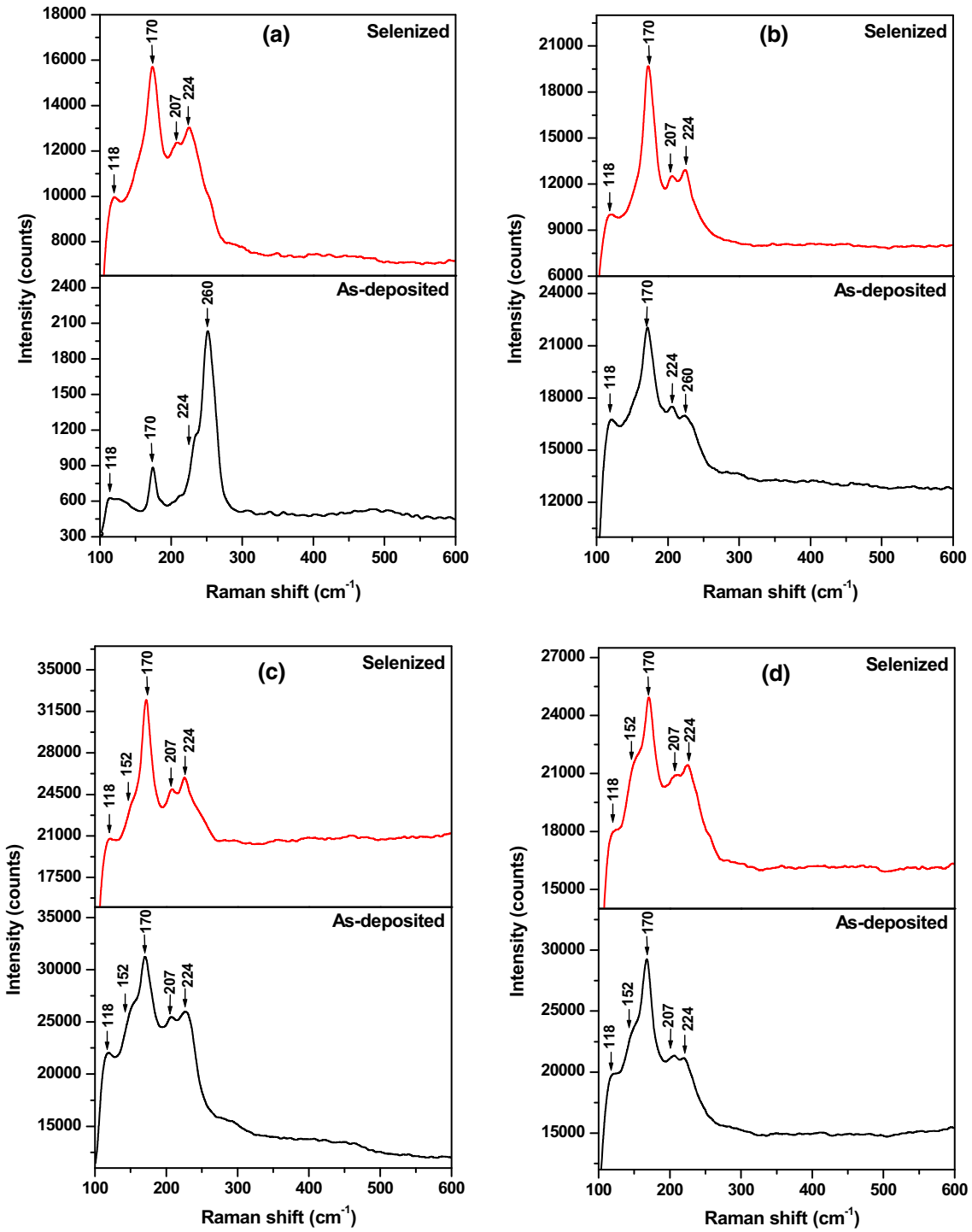

Fig. 4 Raman spectra for CIS thin films deposited at various deposition potentials −0.7 V (**a**), −0.8 V (**b**), −0.9 V (**c**) and −1 V (**d**) on FTO coated glass substrate

respect to deposition potentials was observed. All as-deposited layers were void free, compact and fairly uniform with particle size ∼50 to 200 nm. A part of these films were selenized in tubular furnace at 400 °C for 15 min. The surface morphology of all selenized layers changed, which could be clearly visualized in SEM images. The large globular clusters of size ∼1 micron are formed by agglomeration of small particles. The large clusters have less grain boundaries and useful to produce high efficiency solar cell devices. The cross section SEM micrograph for

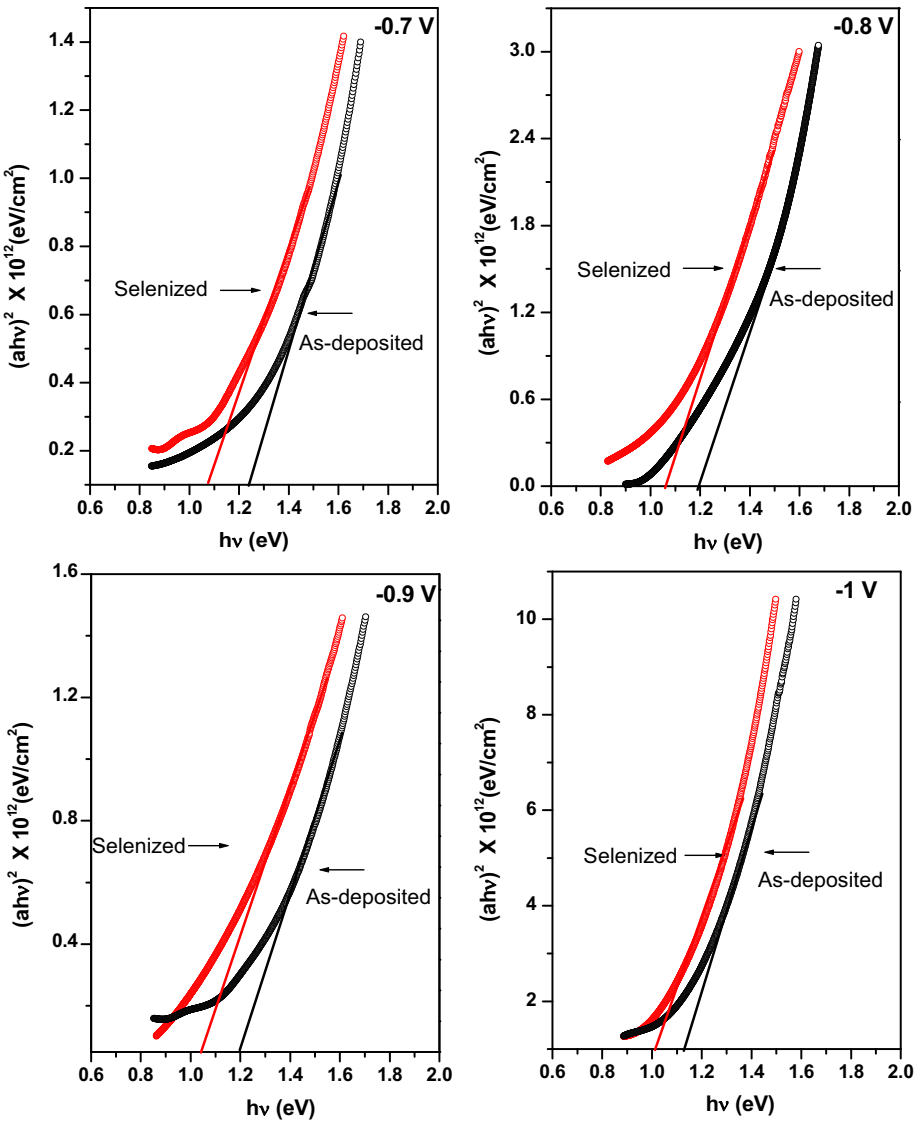

Fig. 5 Optical absorption spectra, $(\alpha h\upsilon)^2$ verses $(h\upsilon)$ for as-grown and selenized CIS thin films prepared at various deposition potentials

Table 2 Band-gap of as-grown and selenized CIS layers electrodeposited at various deposition potentials estimated from optical studies

Deposition potential (V)	Band gap (eV)	
	As-grown	Selenized
−0.7	1.13	1.01
−0.8	1.18	1.04
−0.9	1.20	1.06
−1	1.24	1.08

selenized CIS thin film electrodeposited at −0.8 V is shown in Fig. 6e. The selenized film showed a smooth, homogeneous and compact appearance. The film thickness is about 1.5 μm, excluding big lumps present on the surface. Due to large variation in grain size and layer thickness, the surface is rough. The contrast appeared in all SEM images could be due to the rough surface.

3.4.2 EDAX analysis

The atomic percentage concentration obtained by EDAX analysis for both as-deposited and selenized sample is summarized in Table 3. Figure 7 shows the variation in Cu, In and Se contents determined as a function of applied potentials for the selenized samples. The contents of Cu was found to be reduced systematically with increasing the cathodic deposition potentials and the contents of In were increases for the film deposited at higher growth potentials which agrees with the equilibrium potentials of Cu and In. The contents of selenium in the as-deposited CIS layer were obtained in the range from 40 to 50 at.% of total 100 % of Cu, In and Se. Upon selenization the content of

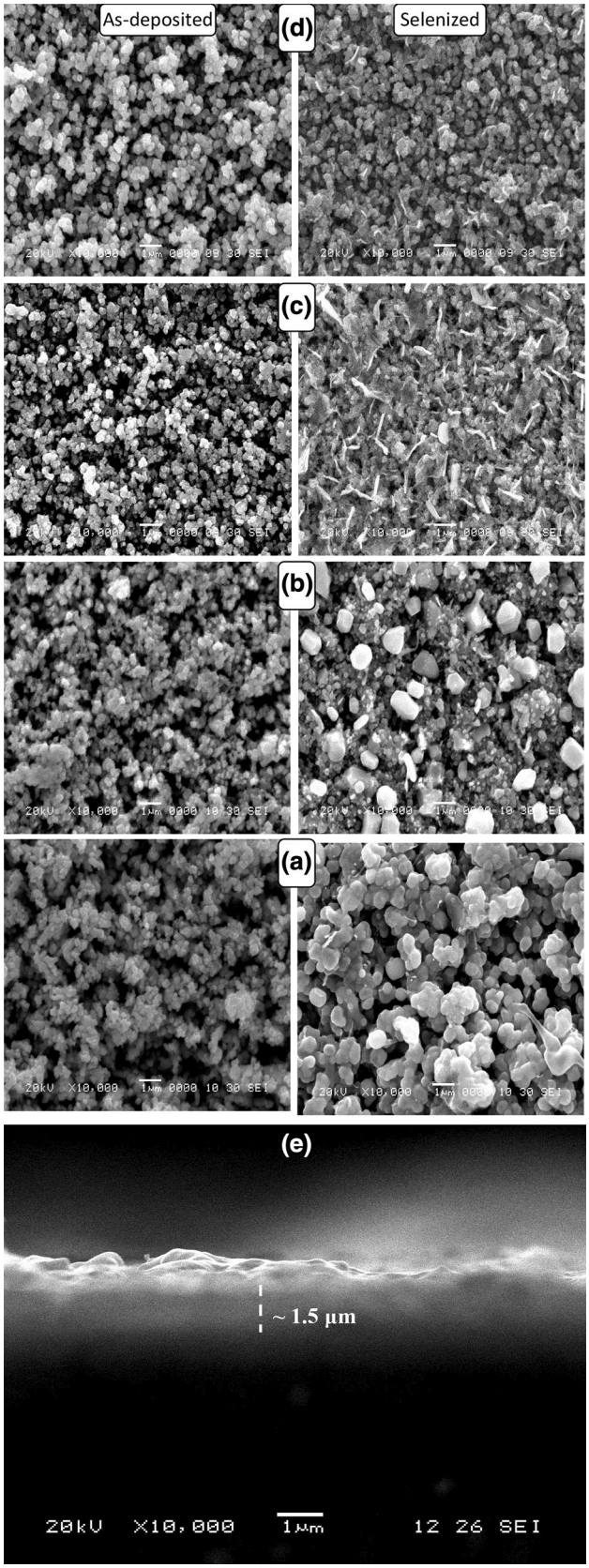

◀**Fig. 6** SEM images of as-grown and selenized CIS thin films deposited for potentials −0.7 V (**a**), −0.8 V (**b**), −0.9 V (**c**), −1 V (**d**) and cross section SEM micrograph for selenized CIS thin film grown at −0.8 V (**e**)

Se were increased up to 50 % close to stoichiometry. The films deposited at −0.7 and −0.8 V were Cu-rich, whereas the In-rich CIS were formed for higher deposition potentials (−0.9 and −1 V). The result obtained by EDAX agrees well with the structural data obtained by XRD and Raman analyses.

3.5 Photo-electrochemical properties

Figure 8 presents the photoresponse curve, photocurrent density verses time for selenized CIS thin films deposited at −0.7 V (c), −0.8 V (d), −0.9 V (e) and −1 V (f) along with the standard n-type silicon (a), p-type silicon (b), under chopped white light illumination of intensity 100 mW/cm^2. The standard p-type and n-type silicon samples of resistivity, 0.05 Ω cm were used as reference. A small bias voltage −10 mV was applied during the PEC measurement. The photocurrent measured for n-type silicon sample upon illumination was found to be increased along the positive direction (Fig. 8a), whereas, the enhancement in the photocurrent along negative direction was noticed for p-type silicon sample (Fig. 8b). Upon illumination the selenized CIS layers deposited at lower cathodic potentials (−0.7 and −0.8 V) the photocurrent increases towards negative direction, confirm the p-type conductivity could be due to presence of more copper contents. The photoresponse measured for selenized CIS films electrodeposited for higher cathodic deposition potentials (−0.9 and −1 V) was found to be increased towards positive direction under illumination indicates the n-type behavior. The n-type behavior observed in selenized CIS thin films can be ascribed to intrinsic defects such as selenium vacancies or binary phases related to In_XSe_Y. A small applied negative bias could extract the electrons from the conduction band, therefore the electrons in the conduction band of p-type semiconductor are negligible [34]. However, upon illumination the transportation of electrons from the valence band to the conduction band takes place, which could further driven to the solid/electrolyte interface and finally transferred to the solution by reduction of the H^+ ions results an enhancement in the cathodic current [35]. The sharp edges observed during ON and OFF of the light indicates the selenized CIS layer may have low defects and could be suitable for the development of high efficiency solar cells.

Table 3 Atomic percentage concentration determined by EDAX analysis

Composition (at.%)	Deposition Potential of CIS films (V) with respect to Ag/AgCl reference electrode			
	−0.7 V	−0.8 V	−0.9 V	−1 V
Copper				
As-grown	29.30	27.39	30.98	21.70
Selenized	29.51	29.08	22.02	19.22
Indium				
As-grown	24.16	28.92	32.55	37.59
Selenized	13.90	19.43	29.90	34.82
Selenium				
As-grown	46.34	43.70	36.77	40.71
Selenized	56.59	50.58	48.08	45.91

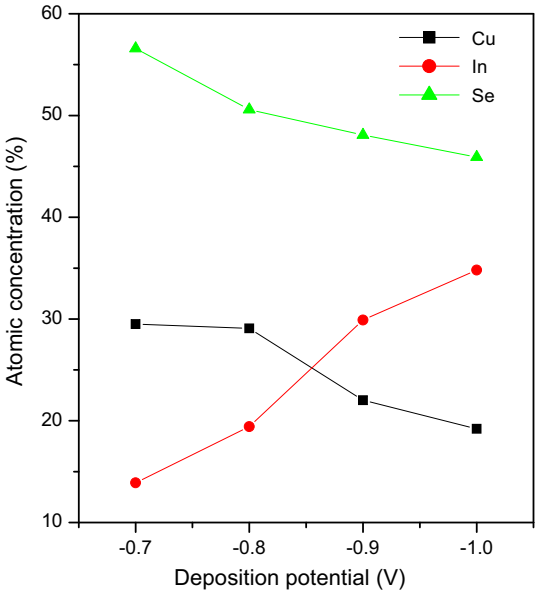

Fig. 7 Plot of Cu, In and Se contents obtained by EDAX analysis for selenized CIS layers deposited for various growth potentials

3.6 Electrical properties

The current density–voltage (J–V) characteristics have been investigated to explore the electrical properties of CIS thin films (not shown here). Au metal contact of diameter 1 mm was made on CIS layer by thermal evaporation technique. A Schottky behavior was observed for as-grown and selenized samples. A semilogarithmic plot, ln (I) versus applied bias (V) of as-grown and selenized CIS films electrodeposited at −0.8 V is depicted in Fig. 9. The value of the ideality factor (η) is calculated from the slope of linear region for the forward bias with the following equation [36].

$$\eta = \frac{q}{kT}\frac{dV}{d(\ln I)} \quad (8)$$

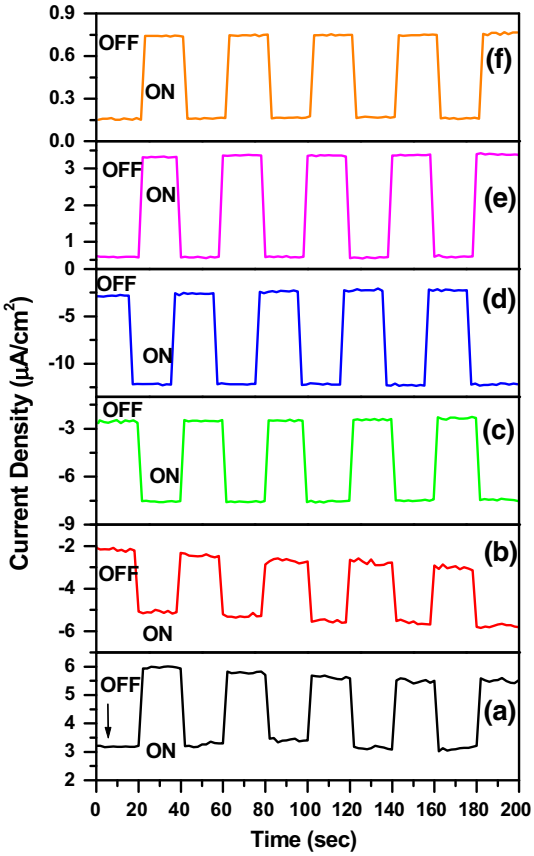

Fig. 8 Photocurrent density versus time curves for standard n-type silicon (*a*), p-type silicon (*b*), selenized CIS thin films deposited at different deposition potentials −0.7 V (*c*), −0.8 V (*d*), −0.9 V (*e*) and −1 V (*f*)

where 'q' is the charge of electron, 'V' is the applied bias, 'η' is the ideality factor, 'k' is the Boltzmann constant, 'T' is the temperature and 'I' the is diode current. The values of ideality factor 'η', 1.73 and 1.15 were calculated for as-grown and selenized CIS thin films. It is evident that the ideality factor calculated for selenized samples is lower

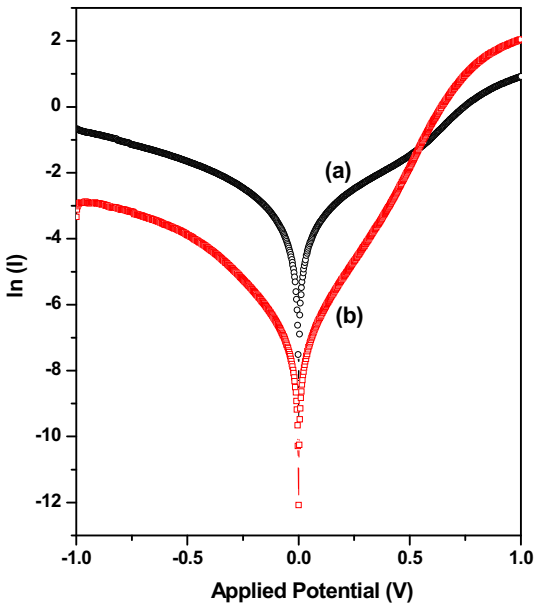

Fig. 9 Plot of ln (I) versus applied bias (V) of as-grown and selenized CIS layers deposited at −0.8 V

than that of the as-grown sample could due to the re-crystallization of the materials which reduces the grain boundaries. The reverse current measured for as-grown could be associated to the structural disorders, such as grain boundaries which may provide high resistive path for the movement of charge carriers.

4 Conclusion

Polycrystalline CIS thin films were successfully electrodeposited from aqueous bath by one-step electrochemical technique. The oxidation and reduction features related to Cu, In and Se were clearly observed in cyclic voltammetry. Chronoamperometric measurement revealed a characteristic of diffusive controlled growth with instantaneous nucleation. Tetragonal chalcopyrite structure was revealed for as-grown and selenized CIS thin film by the X-ray diffraction studies. Highly crystalline CIS layers were formed upon selenization with preferential orientation along (112) plane. The sample grown at −0.8 V attributed to peaks related to CIS without secondary phases. The secondary phases are exhibited for the sample deposited for the potentials deviated from −0.8 V to either side. Raman studies confirm the presence of chalcopyrite phase of CIS. Ordered defect compound (ODC) related peaks were revealed in CIS layers electrodeposited at higher deposition potentials. EDAX analysis confirms the stoichiometric growth of CIS at growth potential −0.8 V, however Cu-rich and In-rich CIS layers were grown at lower and higher deposition potentials, respectively. Optical studies estimated the values of band-gap of selenized CIS ∼1.05 eV. Upon selenization void free with globular surface morphology of cluster size ∼1 to 2 μm layers were obtained. PEC analysis revealed the growth of p-type conductivity layer at lower potentials and n-type conductivity layer at higher growth potentials. Electrical measurements showed the Schottky behavior of CIS layers deposited at various growth potentials. The value of ideality factor decreases upon selenization probably due to the recrystallization of material.

Acknowledgments The financial support received from Defence Research and Development Organization (DRDO), New Delhi under the major project grant ERIP/ER/10003866/M/01/1388 is gratefully acknowledged. ABR also acknowledged CSIR for senior research fellowship.

References

1. M.G. Lakhe, N.B. Chaure, Sol. Energy Mater. Sol. Cells **123**, 122 (2014)
2. M. Gloeckler, J.R. Sites, J. Phys. Chem. Solids **66**, 1891 (2005)
3. A. Antony, A.S. Asha, R. Yoosuf, R. Manoj, M.K. Jayras, Sol. Energy Mater. Sol. Cells **81**, 407 (2004)
4. M.A. Green, K. Emery, Y. Hishikawa, W. Warta, E.D. Dunlop, Solar cell efficiency tables (version 45). Prog. Photovolt. Res. Appl. **23**, 1 (2015)
5. I. Repins, M. Contreras, B. Egaas, D. Clay, J. Scharf, C. Perkins, B. To, R. Noufi, Prog. Photovolt. Res. Appl. **16**, 235 (2008)
6. H. Lee, W. Lee, J. Kim, M. Ko, K. Kim, K. Seo, D. Lee, H. Kim, Electrochim. Acta **87**, 450 (2013)
7. N.B. Chaure, J. Young, A.P. Samantilleke, I.M. Dharmadasa, Sol. Energy Mater. Sol. Cell **81**, 125 (2004)
8. L. Ribeaucourt, G. Savidand, D. Lincot, E. Chassaing, Electrochim. Acta **56**, 6628 (2011)
9. N.D. Nikolić, K.I. Popov, L.J. Pavlović, M.G. Pavlović, J. Electroanal. Chem. **588**, 88 (2006)
10. N.B. Chaure, R. Jayakrishnan, J.P. Nair, R.K. Pandey, Semicond. Sci. Technol. **12**, 1171 (1997)
11. N.B. Chaure, S. Chaure, R.K. Pandey, Electrochim. Acta **54**, 296 (2008)
12. N.B. Chaure, J. Renew. Sustain. Energy **5**, 031604 (2013)
13. N.B. Chaure, A.P. Samantillleke, R.P. Burton, J. Young, I.M. Dharmadasa, Thin Solid Films **472**, 212–216 (2005)
14. P.U. Londhe, A.B. Rohom, N.B. Chaure, J. Mater. Sci. Mater. Electron. **25**, 4643 (2014)
15. A.B. Rohom, P.U. Londhe, N.B. Chaure, J. Solid State Electrochem. **19**, 201 (2015)
16. M.G. Lakhe, S.K. Mahapatra, N.B. Chaure, Mater. Sci. Eng. B (2015). doi:10.1016/j.mseb.2015.11.005
17. J.P. Nair, R. Jayakrishnan, N.B. Chaure, S. Gohkale, A. Lobo, S.K. Kulkarni, R.K. Pandey, J. Phys. Chem. Solids **60**, 1693 (1999)
18. P.U. Londhe, A.B. Rohom, N.B. Chaure, RSC Adv. **5**, 89635–89643 (2015)
19. R.N. Bhattacharya, J. Electrochem. Soc. **130**, 2040 (1983)
20. D. Pottier, G. Maurin, J. Appl. Electrochem. **19**, 361 (1989)
21. J.F. Guillemoles, P. Cowache, A. Lusson, K. Fezzaa, F. Boisivon, J. Vedel, D. Lincot, J. Appl. Phys. **79**, 7293 (1996)

22. D. Lincot, J.F. Guillemoles, P. Cowache, S. Massaccesi, L. Thouin, K. Fezzaa, F. Boisivon, J. Vedel, in *Proceedings of the First World Conference and Exhibition on Photovoltaic Solar Energy Conversion*, vol. 136 (1994)
23. S.N. Qiu, L. Li, C.X. Qiu, I. Shih, in *Proceedings of the 12th European Photovoltaic Solar Energy Conference. Stephens Bedford*, vol. 1539 (1994)
24. M.G. Ganchev, K.D. Kochev, Sol. Energy Mater. Sol. Cells **31**, 163 (1993)
25. R.N. Bhattacharya, W. Batchelor, H. Wiesner, F. Hasoon, J.E. Granata, K. Ramanathan, J. Alleman, J. Keane, A. Mason, R.J. Matson, R.N. Noufi, J. Electrochem. Soc. **145**, 3435 (1998)
26. R.N. Bhattacharya, M. Oh, Y. Kim, Sol. Energy Mater. Sol. Cell **98**, 198 (2012)
27. R.N. Bhattacharya, A.M. Fernandez, Sol. Energy Mater. Sol. Cells **76**, 331 (2003)
28. A.J. Bard, L.R. Faulkner, *Electrochemical Methods Fundamentals and Applications*, 2nd edn. (Wiley, New York, 2001)
29. A. Chao, S. Ahn, J.H. Yun, J.G. Wak, S.K. Ahn, K. Shin, H. Song, K.H. Yoon, Sol. Energy Mater. Sol. Cells **109**, 17 (2013)
30. H. Zhao, M. Kumar, G. Persson, Phys. Status Solidi C **9**, 1600–1603 (2012)
31. W. Witte, R. Knise, M. Powalla, Thin Solid Films **517**, 867–869 (2018)
32. R. Marquez, C. Rincon, Sol. Energy Mater. Sol. Cell **71**, 19–26 (2002)
33. O. Ramadani, J.F. Gulliemoles, D. Loncot, P.P. Grand, E. Chassing, O. Kerrac, E. Rzepka, Thin Solid Films **515**, 5909 (2007)
34. R. Memming, *Semiconductor Electrochemistry*, vol. 167 (Wiley, Weinheim, 2001)
35. C. Guillen, J. Herrero, Sol. Energy Mater. Sol. Cells **73**, 141 (2002)
36. S. Gupta, D. Patidar, N. Saxena, K. Sharma, Chalcogenide Lett. **6**, 723 (2009)